

## Scanning tunneling microscope studies of the superconductor proximity effect

Y. Levi and O. Millo\*

*Racah Institute of Physics, the Hebrew University, Jerusalem 91904, Israel*

N. D. Rizzo<sup>†</sup> and D. E. Prober

*Applied Physics, Yale University, New Haven, Connecticut 06520-8284*

L. R. Motowidlo

*IGC-AS, Waterbury, Connecticut 06704*

(Received 29 June 1998)

Scanning tunneling microscopy and spectroscopy are employed in studies of the proximity effect between normal metals and superconductors. The experimental configuration is unique, in that the tunneling current flows in parallel to the interfaces between different materials. The samples are superconducting wires consisting of ordered arrays of submicron diameter normal-metal filaments, either Cu or Ni (a ferromagnet), embedded in a NbTi superconducting matrix. By taking topographic images simultaneously with current-voltage curves, we map with nanometer resolution the local quasiparticle density of states. Two main issues are addressed in this work. The first is the spatial variation of the superconductor gap as a function of distance from the boundary between the normal-metal and the superconductor. We find that the healing length of the gap on the superconducting side is much larger than the superconductor coherence length. The second is the observation of pronounced Tomasch oscillations and bound states arising from multiple Andreev reflections of quasiparticles propagating in the plane perpendicular to the tunneling current. [S0163-1829(98)03946-0]

### INTRODUCTION

The mutual influence of a superconductor ( $S$ ) in electrical contact with a normal metal ( $N$ ), a phenomenon known as the proximity effect (PE), has been studied extensively in the past three decades.<sup>1,2</sup> Among the main issues that are dealt with when addressing the PE are the following: (1) Spatial variations of the pair amplitude in the vicinity of the  $S$ - $N$  boundary. (2) Quasiparticle bound and resonant states arising from multiple Andreev reflections at  $S$ - $N$  interfaces in structures comprising more than a single such boundary. These effects are reflected in the local quasiparticle density of states (DOS) that can be measured in a tunneling experiment, in particular using a scanning tunneling microscope (STM) with a normal metal tip. At  $T=0$ , the measured tunneling  $dI/dV$  vs  $V$  curve is directly proportional to the sample's DOS, and at finite temperatures it is thermally smeared. In a conventional BCS bulk superconductor the DOS has the form  $|E|/\sqrt{E^2-\Delta^2}$  for  $|E|>\Delta$  and zero for  $|E|<\Delta$ , where  $\Delta$  is the gap parameter and equals half the energy gap in the DOS. In a homogeneous  $S$ , the gap coincides with the superconducting pair potential,  $\Delta_p$ , responsible for the condensation of quasiparticles into Cooper pairs.<sup>3</sup> In a  $N$ - $S$  proximity structure, where  $\Delta_p$  is not spatially uniform, the gap in the DOS and the pair potential do not necessarily coincide. Ideally, an abrupt change in the pair potential is assumed: from a finite  $\Delta_p$  on the  $S$  side, to zero on the  $N$  side. However, the DOS (which can be measured experimentally) changes smoothly from the  $N$  side to the  $S$  side, due to the smooth variations of the pair amplitude, which describes the correlations between electrons of opposite spins. The pair amplitude can be inferred from the spatial variations in the DOS, using Usadel formalism,<sup>4</sup> as was done by Gueron *et al.*<sup>5</sup> and

Belzig, Bruder, and Schoen.<sup>6</sup> A measure for the pair amplitude can also be obtained from the magnitude of the gap (or ‘‘minigap’’ in Refs. 5 and 6) in the DOS. The gap  $\Delta$  can be extracted by fitting the measured DOS to the Usadel equations.<sup>5,6</sup> However, at a region close enough to the  $S$ - $N$  interface, a good estimate for the gap can be obtained by fitting to a lifetime broadened BCS DOS, such as was introduced by Dynes, Naraynamurti, and Garno.<sup>7</sup> Thus, spatially resolved measurements of the DOS are fundamental in order to study the spatial variations of the pair amplitude in PE structures.

Recently, research of the PE gained further momentum thanks to technological advances that enable the fabrication of complex mesoscopic devices. Nevertheless, many of these works<sup>8-11</sup> followed earlier studies<sup>2</sup> and addressed macroscopic properties of the samples, thus obtaining average rather than local information on the DOS. In other cases<sup>5</sup> spatially resolved data were sought, but only in a limited number of locations. The advent of STM enables spatially resolved measurements of the DOS. This is achieved by taking topographic images simultaneously with tunneling current-voltage ( $I$ - $V$ ) or  $dI/dV$  vs  $V$  characteristics. Some STM experiments treated systems composed of a normal-metal island film deposited onto a  $S$  substrate.<sup>12,13</sup> In these works tunneling took place *perpendicular* to the  $S$ - $N$  interface, so that the evolution of the DOS as a function of distance from the  $S$ - $N$  boundary was not deduced. Hess *et al.* measured a type-II superconductor in the Abrikosov vortex lattice state, mapping the DOS around and within a single flux-vortex.<sup>14</sup> Although in these experiments tunneling was in parallel to the ‘‘boundaries’’ between  $N$  and  $S$  regions, this STM study did not address a proximity structure involving *different* metals. Inoue and Takayanagi employed STM to

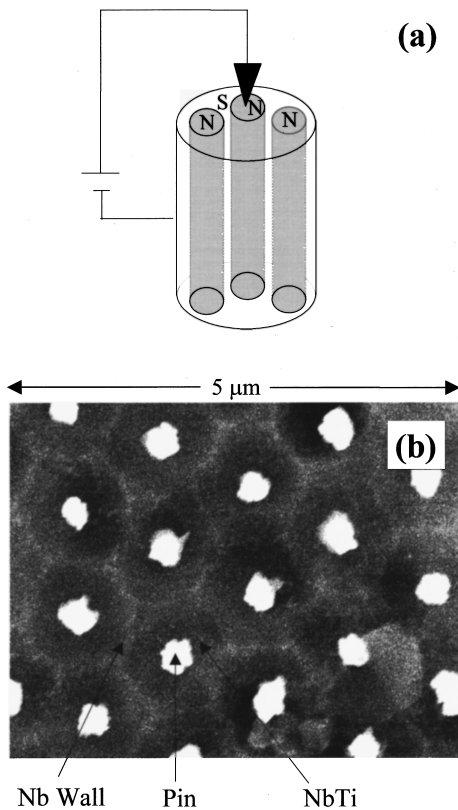


FIG. 1. (a) Schematic of the experimental setup. The black arrow represents the STM tip, and tunneling takes place in parallel to the interfaces between the wire's constituents. (b) Scanning electron microscope micrograph of a large Ni island-pin wire, sample A, displaying an array of unit filaments. Each unit filament consists of a pin (bright), surrounded by a NbTi hexagon (dark) that is coated by a thin Nb layer (bright).

study the evolution of the DOS as a function of the lateral distance from a  $S$ - $N$  interface, where the  $S$  was a thin overlayer film.<sup>15</sup>

In our research we employ a cryogenic STM in order to obtain *spatially resolved* information about the local quasiparticle DOS, when tunneling parallel to the material boundaries. The samples consist of ordered arrays of  $S$  and  $N$  filaments of “semi-infinite” length in good electrical contact, where the arrays have a lateral scale in the submicron range. This lateral scale is suitable for STM studies, and also enables the observation of mesoscopic effects resulting from multiple Andreev reflections. Furthermore, in some samples the  $N$  metal is ferromagnetic, and as such is inimical to superconductivity, so that a pronounced proximity effect is expected. A schematic illustration of the experimental configuration is shown in Fig. 1(a).

We focus on two properties of these systems: (a) The evolution of the DOS as a function of the distance from the  $S$ - $N$  boundary; preliminary results on this issue have already been published,<sup>16</sup> and here we present further studies performed on samples of a different lateral scale, which allow a better understanding of the data. (b) Evidence of bound states (of the de Gennes–Saint James type)<sup>2,17</sup> and Tomash oscillations<sup>2,18</sup> observed at specific STM tip locations over the sample. The latter measurements are unique in that tunneling occurs perpendicular to the plane where the quasipar-

ticles that undergo Andreev reflections propagate (and in parallel to the reflecting planes).

The samples we investigate are “artificial pinning centers (APC's) wires” manufactured at IGC-Advanced Superconductors. APC superconducting wires are specially engineered to enhance magnetic-flux pinning in order to increase the critical current at high magnetic fields. While in the conventional technique flux pins are introduced by creating random defects along the wire, the APC approach introduces chosen pin materials in a well-defined ordered filamentary configuration. These wires have already demonstrated higher critical currents than those produced with conventional processing.<sup>19,20</sup> Details of the fabrication process and of the wires' electrical properties at various magnetic fields are reported elsewhere.<sup>19</sup> In order to further optimize the performance of these wires, local measurements such as those reported here are needed. Thus, our work has also technological importance and demonstrates the effectiveness of STM in applied research.

## EXPERIMENT

We used three types of APC wires. The first two have the “island”-pin geometry and use a Cu-coated ferromagnetic (Ni) pin. The Cu sleeve serves as a diffusion barrier against the migration of Ni into NbTi. The “unit filament” consists of a pin placed inside a NbTi ( $S$ ) cylinder that is surrounded by a thin Nb cylinder [ $S'$  in Fig. 4(a)]. After some steps of extrusion, drawing, and restacking, where only the first step is performed at elevated temperature (“hot step”), the wires are reduced by drawing to their final size. We studied two types of Ni island-pin wires. Sample A: “Large wire” [Figs. 1(b), 3(a), 4], where each unit filament has an outer diameter of  $1.3 \mu\text{m}$ , and the pin consists of a cylindrical Ni filament 200 nm in diameter, surrounded by a 50 nm thick Cu sleeve. A scanning electron microscope (SEM) micrograph taken on sample A displaying part of an array of individual Ni island pins is shown in Fig. 1(b). Sample B: “Small wire” [Figs. 2, 3(b)], which is derived from the large wire by an additional cold draw step. All the lateral dimensions of this wire are reduced by one order of magnitude with respect to sample A. The third wire, sample C, [Figs. 3(c) and 5] has the “barrier-pin” geometry, where the unit filament is a NbTi hexagon 80 nm in size, surrounded by a 15 nm thick Cu cladding, making the distance between adjacent superconducting filaments 30 nm. The Cu cladding serves as the pin. The parameters of all three samples are summarized in Table I. This choice of wires allows the study of samples with different geometries and lateral dimensions. It also affords a comparison between samples having ferromagnetic constituents as opposed to ones that are nonmagnetic.

Sample preparation for STM measurements consists of cutting the wires, polishing them along their cross section and finally subjecting them to a short chemical etch. Besides removing surface impurities and oxide layers, the chemical process causes some of the constituents to be more depressed relative to others (due to different etch rates), and thus facilitates the STM detection of the boundaries between different materials. Immediately after the etch the samples are mounted onto our cryogenic STM, having a Pt-Ir (normal

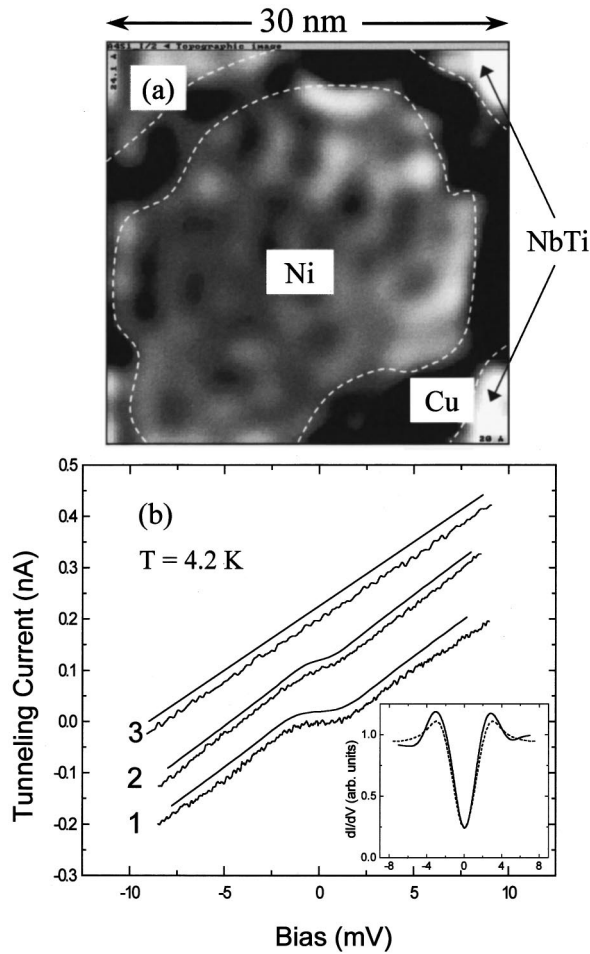


FIG. 2. (a) STM topographic image taken on a small Ni island-pin wire, sample *B*, depicting an individual Ni pin. Most of the Cu sleeve is visible around the pin. The interfaces between the different constituents have been designated by dashed lines. (b) Three  $I$ - $V$  characteristics taken at 4.2 K at different lateral tip positions on sample *B*. The curves were taken deep in the NbTi, on the Cu and on the Ni, respectively, for curves 1–3. The smooth lines were calculated using Dyne’s formula (Ref. 7). For curves 1–3, the gaps are 1.55, 0.85, and 0 meV, respectively. Curves are displaced for clarity. Inset: a  $dI/dV$  trace taken deep in the NbTi region. The dotted line is a theoretical fit to Dynes’ formula, with a gap of 1.55 meV.

alloy) tip. The sample space is then evacuated and filled with low-pressure He exchange gas, prior to immersing it in liquid helium. All the data presented in this paper were acquired at a temperature of 4.2 K.

STM topographic images of the wire cross section were taken simultaneously with  $I$ - $V$  or  $dI/dV$  vs  $V$  characteristics at different lateral tip positions. The  $I$ - $V$  and derivative curves were acquired while momentarily disabling the STM feedback loop. The local DOS vs energy was thus studied (via the  $dI/dV$  vs  $V$  curves) in correlation with the surface structure. The differential conductance curves were either measured directly using standard lock-in technique, or by numerical differentiation of the acquired  $I$ - $V$  curves. Care was taken to use small enough tunneling currents so that local superconductivity, in particular the measured DOS, was unaffected.

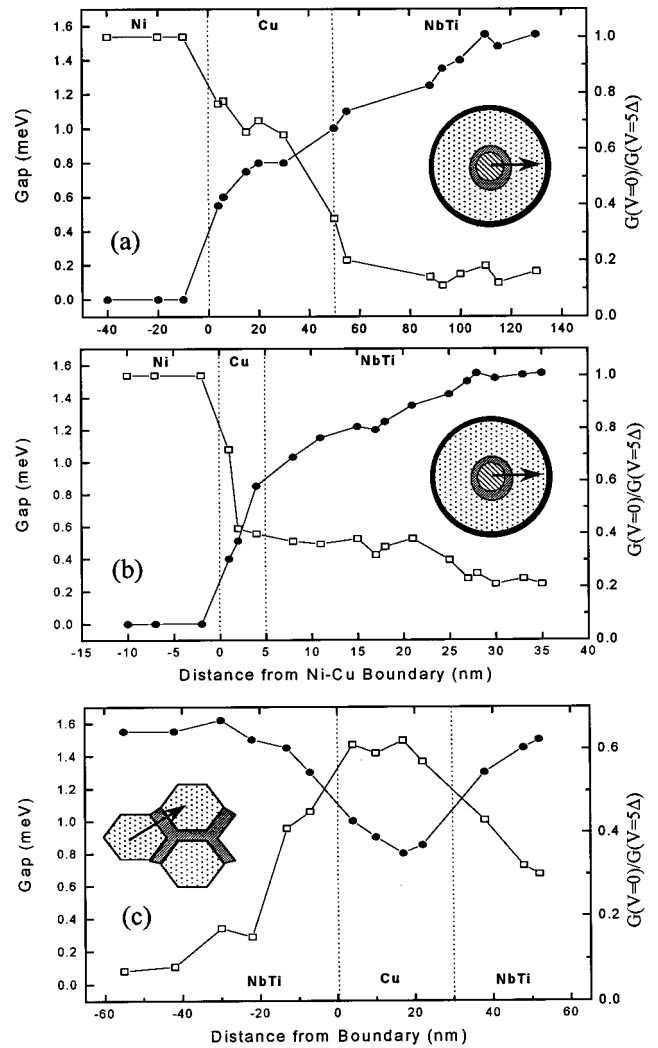


FIG. 3. (a) Gap (black circles, left axis) and normalized ZBC (white squares, right axis) on the large Ni island-pin wire, sample *A*, as a function of distance from the Ni-Cu interface. Boundaries between different types of materials are designated by vertical dashed lines. The experimental errors on the data are approximately the size of the symbols. Inset: Diagram of the area studied, with an arrow illustrating the scan line on which the  $I$ - $V$  curves were taken. (b) Same as (a), but for the small Ni island-pin wire, sample *B*. Note that the horizontal scale is much smaller. (c) The same as (a), but for the Cu barrier-pin wire, sample *C*. Note the different horizontal scale and that the scan line crosses two NbTi/Cu boundaries.

## RESULTS AND DISCUSSION

### Spatial variations of the superconducting gap, $\Delta$

In Fig. 2(a) we present a topographic image taken on the small Ni island-pin wire, sample *B*. The topographic scan was performed with a bias of 50 meV, well above the superconducting gap of NbTi, where the local DOS in  $S$  is “metallic” (constant). Thus, the image represents the true surface topography of the sample. The image focuses on an individual pin, with parts of the Cu sleeve and NbTi also showing (depressed, due to a faster etch rate). Dashed lines were drawn along the different boundaries, which can be determined from the image to an accuracy of the order of 1 nm. The image is presented in gray scale, where dark corresponds to depressed areas and bright to elevated ones. This is in

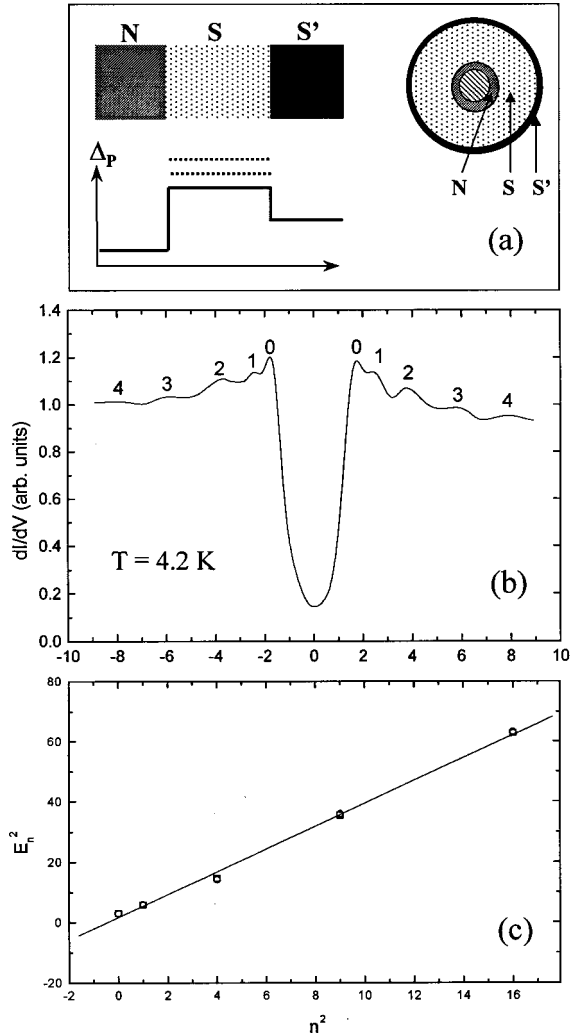


FIG. 4. (a) Left: An illustration of the variation of the pair potential  $\Delta_p$  at the boundaries between different materials. Such a configuration can give rise to resonant states (dashed lines), and Tomasch oscillations in the  $I$ - $V$  curves. Right: A schematic of a Ni island-pin unit filament, where this configuration is realized;  $N$ (Cu),  $S$ (NbTi),  $S'$ (Nb). (b) A  $dI/dV$  vs  $V$  curve taken on a large Ni island-pin wire, sample A, with the STM tip situated on the NbTi, in the vicinity of the Cu-NbTi interface. Notice the four peaks above the gap edge ("0"), attributed to Tomasch oscillations. (c) The energy squared of the peak positions plotted as a function of the square of peak number, designated in (b). The nearly overlapping symbols correspond to peaks at negative (circles) and positive (squares) bias. The data points fall nearly on a straight line, from which one can obtain, using Eq. (1), the pair potential and the width of the superconductor: 1.3 meV and 510 nm.

contrast to a SEM image, such as Fig. 1(b), where bright areas signify enhanced secondary electron emission. When comparing Fig. 1(b) (sample A) to 2(a) (sample B) one should also note the differences in lateral scales and spatial (three dimensional) resolution. In Fig. 2(b) we plot three experimental  $I$ - $V$  curves and corresponding fits (smooth lines), taken at different positions on sample B, manifesting the changes in the local DOS. In curve 1, taken deep inside the superconductor, a large gap in the DOS is apparent. Curve 2 was acquired inside the Cu, where the gap is much smaller, but nevertheless clearly observed. The gap in Cu

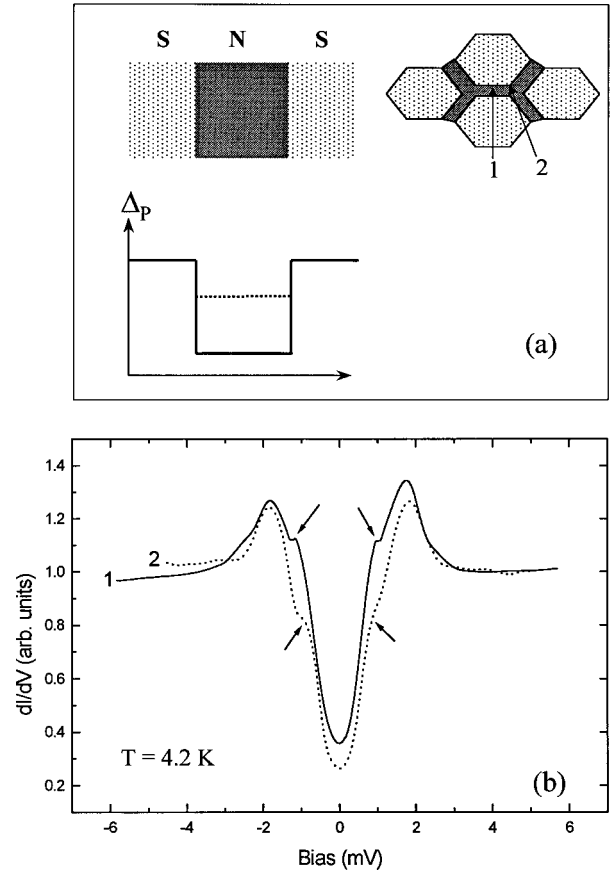


FIG. 5. (a) Left: An illustration of the variation of the pair-potential  $\Delta_p$  at two different boundaries between  $N$  and  $S$ . This configuration can support quasiparticle bound states (dashed line). Right: A schematic of the unit filament in the Cu barrier-pin wire, sample C, where such a configuration is realized;  $N$ (Cu),  $S$ (NbTi). (b) Two normalized  $dI/dV$  vs  $V$  curves taken on a Cu barrier-pin wire, on the Cu, in the vicinity of the NbTi-Cu interface. The curves were acquired at two different positions, as indicated in (a). Both curves exhibit a subgap structure (highlighted by arrows) at energies consistent with the presence of bound states.

should not be confused with the local pair potential,  $\Delta_p$ , which is vanishingly small in Cu.<sup>2</sup> Inside the Ni, where curve 3 was measured, the gap vanishes completely, and the  $I$ - $V$  characteristic is Ohmic. In the inset we plot a typical derivative curve acquired well within the NbTi along with a theoretical fit (dashed line). This curve too exhibits a pronounced gap structure, manifesting a gap in the DOS. We note that when the wires were measured at  $\sim 10$  K (just above  $T_C \approx 9$  K), only gapless curves were found all over the sample. This indicates that the gaps in the DOS present at 4.2 K (both in NbTi and in Cu) are due to superconductivity and not to extraneous effects.

Two main parameters can be extracted from the curves: the magnitude of the gap in the DOS and the zero-bias conductance (ZBC) normalized to the conductance at a high bias. The occurrence of a large gap combined with low ZBC is a signature of superconductivity (large pair amplitude) at that location, while a small or vanishing gap, together with a normalized ZBC close to unity, signify normal metallic behavior. In order to extract the gap we fit the data to the conventional tunneling expressions for  $N$ -insulator- $S$  tunnel

TABLE I. Type and dimensions of the three wires studied. The thickness of NbTi and Cu for samples *A* and *B* refer to the widths of the cylinders, not their outer diameter. In sample *C* the Cu thickness refers to the width of the wall which separates two adjacent NbTi filaments. The rightmost column presents the healing length of superconductivity inside the NbTi, as explained in the text.

Sample	Type of wire	Ni diameter (nm)	Cu thickness (nm)	NbTi thickness (nm)	Healing length (nm)
<i>A</i>	Large Ni island	200	50	500	60–70
<i>B</i>	Small Ni island	20	5	50	25
<i>C</i>	Cu Barrier		30	80	25

junctions,<sup>2</sup> taking the DOS introduced by Dynes *et al.*<sup>7</sup> Such fits (performed for  $T=4.2$  K) are presented in Fig. 2(b). One can see that the fits are satisfactory when trying to depict the gross behavior of the curves, in particular the gap. However, this approach cannot account for additional structures that may appear, either within or above the gap region (as will be discussed below). A more complete approach for analyzing the variation of the local DOS, in particular in  $N$ , should be within the framework of the Usadel equations.<sup>4,5,6,11,21</sup> Here, however, the distances from the  $N$ - $S$  boundary where our data were acquired are much smaller than the Ginzburg-Landau coherence length in  $N$ ,  $\xi_N$  (typically  $\sim 100$  nm at 4.2 K). At this range the Usadel DOS does not deviate significantly from the one used in Dynes' model.

Figures 3(a), 3(b), and 3(c) show the variations of the gap and the ZBC as a function of the distance from the boundaries for the three wires. The insets illustrate the direction along which the  $I$ - $V$  curves were taken, and the various metals along that line. For the large Ni island pin, sample *A* [Fig. 3(a)], one can see that the curves taken inside the Ni are Ohmic, but in the Cu sleeve, *adjacent to the Ni*, indications of a gap are already found. As the NbTi is approached from inside the Cu, the gap increases and the ZBC diminishes. This trend continues inside the NbTi with growing distance from the pin, and at  $\sim 60$  nm from the NbTi-Cu interface the gap parameter saturates at 1.55 meV (the established<sup>2</sup> value for bulk NbTi) and the ZBC at 0.15. The situation is qualitatively similar for the small Ni island pin, sample *B* [Fig. 3(b)], the only difference being the lateral scale. The healing length for this wire, namely the distance from the NbTi-Cu interface over which the gap attains its bulk value, is found to be shorter, about 25 nm. In the Cu barrier-pin wire, sample *C* [Fig. 3(c)], superconductivity is monotonically suppressed in the NbTi as the Cu-NbTi interface is approached. The gap continues to decrease within the Cu region, reaching its minimal value approximately midway between the two adjacent  $S$  filaments, as expected. The healing length in NbTi in this case is found to be  $\sim 25$  nm. The healing lengths for all three samples, whose determination was made more accurate and reproducible by looking at polynomial fits to our data, are listed in Table I.

It is important to stress here that the healing lengths found for all three wires are significantly larger than the superconducting coherence length expected for NbTi at 4.2 K,  $\xi_S \sim 5$  nm.<sup>22</sup> A possible explanation for this effect could be material intermixing. Although care was taken to design the wires with immiscible materials, it is probable that during wire fabrication, in particular in the hot step, some material interdiffusion may have occurred at the boundaries between different metals. This would result in "blurring" the inter-

faces. However, this does not seem to be the full explanation. The reason being, that since only a cold-step (cold draw) is used to transform a large Ni island-pin wire to a small one, no further significant intermixing is expected. Thus, one would expect the original intermixing present in the large wire (due mainly to the hot-step) to scale down by an order of magnitude from sample *A* to sample *B*. This is not what was found experimentally, where the healing length was reduced only by 60%. Another possible cause for the large healing length, at least in the Ni island-pin wire, could be the presence of the magnetic constituent. Albeit the Ni filaments are not macroscopically magnetized throughout the whole length of the wire, they are divided into magnetic domains, which may be up to 100 nm long.<sup>23</sup> It is plausible that the domain closest to the surface exerts a small magnetic field that may locally degrade superconductivity. The enhanced healing length may also result from a more fundamental reason, the possible reduction of the local pair potential,  $\Delta_p$  in  $S$  near the  $N$ - $S$  interface. To verify this, a self-consistent calculation, where  $\Delta_p$  is allowed to vary smoothly (rather than abruptly) at the interface, may be needed.

The origin and in particular the value of the gap do not lend themselves to an easy interpretation, in particular not in  $N$ . Close to the interface the gap may be affected by intermixing. However, far enough from the boundary, where intermixing effects are negligible, the gap in  $N$  is probably due mainly to Andreev reflections leading to leakage of Cooper pairs and quasiparticles from  $S$  to  $N$ . This is consistent with the dirty-limit approximation for the PE,<sup>2</sup> yielding a Cooper pair (pair amplitude) penetration length of  $\sim 100$  nm into the Cu at 4.2 K, when no magnetic constituents are present [e.g., Fig. 3(c)]. It is also consistent with the fact that the gap is completely suppressed in the ferromagnetic Ni region, at least more than 1 nm away from the Cu-Ni boundary, due to pair breaking. Indeed, the expected coherence length in a ferromagnet is less than a nm.<sup>24,25</sup> Pair breaking results also in a reduction of the penetration length in the Cu, as can be clearly seen in sample *B*, where the Cu sleeve is very thin. These issues are best dealt with (in diffusive systems) using the Usadel formalism.<sup>5,6</sup> It predicts that the coherence between electronlike and holelike quasiparticles of low excitation energies extends over large distances, resulting in the appearance of a "minigap" in the DOS of  $N$ , even at distances significantly larger than  $\xi_N$ . Minigaps at such large distances were observed by Gueron *et al.*<sup>5</sup> In our experiment we focus on the DOS at much smaller distances.

#### Quasiparticle bound states and Tomasch oscillations

Our samples consist of a multitude of  $S$ - $N$  interfaces. Such a configuration may support, in favorable cases, quasi-

particle bound and resonant states, resulting from multiple Andreev reflections.<sup>2,11,17,18</sup> We shall first focus on the resonant states that give rise to Tomasch oscillations. If a superconductor is placed in between two metals having a different pair potential, the structure results in a pair potential step. Quasiparticles having energies above the pair potential that undergo double Andreev reflections at opposing boundaries give rise to resonant states. These resonances are reflected in the  $dI/dV$  vs  $V$  (differential conductance) curves as Tomasch oscillations.<sup>2,18</sup> Theoretical calculations for a one-dimensional structure yield the energy of the  $n$ th conductance peak,

$$E_n^2 \approx \Delta_p^2 + \left( \frac{\hbar v_F}{2d_S} \right)^2 n^2, \quad (1)$$

where  $d_S$  and  $\Delta_p$  are the width of the superconductor and its pair potential, respectively.  $v_F$  is the renormalized (due to strong-coupling effects)<sup>2</sup> Fermi velocity in the superconductor,  $\sim 10^8$  cm/s in NbTi.<sup>2</sup>

A case of Tomasch oscillations appears in the Ni island-pin wires, as shown schematically in Fig. 4(a). The thick NbTi cylinder is placed between the inner Cu sleeve and the outer Nb layer. Andreev reflections can then take place at the Cu-NbTi and NbTi-Nb interfaces. Although Nb and NbTi have a similar  $T_c$ , the gap of NbTi is larger due to strong-coupling effects.<sup>2</sup> (Note, that the pair potential step at the Nb-NbTi interface is not essential for the observation of Tomasch oscillations, since the surface of the unit filament could also serve as an Andreev-reflecting boundary. However, this potential step probably enhances the effect.<sup>2</sup>) Figure 4(b) presents a differential conductance curve taken on the Ni island wire with large pins, sample A, when the tip was placed over the NbTi *near* the NbTi-Cu boundary. Tomasch oscillations, comprising the above-gap structure in the curve, are clearly visible both at positive as well as at negative biases. These oscillations could be observed whenever the interfaces appeared sharp in the STM image. In contrast, no subgap structures appeared in any of the  $I$ - $V$  curves measured on this sample.

These oscillations cannot be attributed to phonon structure, which is found in NbTi only at energies above 10 meV.<sup>2</sup> Nevertheless, in order to prove that they are indeed due to resonant states, and not due to other effects, we plot in Fig. 4(c) the square of the conductance-peak energies ( $E_n^2$ ) vs  $n^2$  [the corresponding integers  $n$  are denoted in Fig. 4(b)]. The data can be well fit to a straight line (shown in the figure), from which  $\Delta_p$  and the width of the superconductor may be extracted using Eq. (1). For the data presented here these values are  $\Delta_p = 1.3$  meV and  $d_S = 510$  nm, and in all the other conductance curves that exhibited Tomasch oscillations, taken on different wires of this type at various locations, we found  $1.2 \leq \Delta_p \leq 1.8$  meV and  $490 \leq d_S \leq 520$  nm. These values of  $\Delta_p$  are consistent with the measured gap in the bulk of Nb (namely, the pair potential in NbTi) and those of  $d_S$  are in close agreement with the nominal thickness of NbTi in this sample, 500 nm. The fact that the Tomasch oscillations appear clearly in our curves is somewhat surprising. Obviously, electrons do not travel ballistically across the 500 nm thick NbTi cylinder, as assumed in the conventional model. However, the detection of Tomasch oscillations sug-

gests a measurable contribution from electrons travelling phase coherently between boundaries. This condition is possibly sufficient for the observation of Tomasch oscillations; a full explanation may require new theoretical calculations.

Further evidence that supports the assignment of the above-gap structure to Tomasch oscillations is that they could be observed only in the NbTi, but not inside the Cu. Furthermore, these oscillations were not seen deep inside the S, but only *near* the S-N boundary, where Andreev reflections take place. Although one might expect to find Tomasch oscillations also in the small Ni island pin, we could not observe them there. This is because in these wires the width of the superconductor is much smaller, and consequently the (expected) resonant states lie at much higher energies [see Eq. (1)], where the probability to undergo Andreev reflections is extremely small. We did find, however, evidence for the first two lowest resonant states (two Tomasch oscillations) in the Cu barrier-pin wires, where the NbTi dimensions are intermediate between the large and small island-pin wires.

Next we discuss the quasiparticle bound states. When a normal metal is placed in between two superconductors, a pair potential well is formed. This potential well may support one or more quasiparticle bound states.<sup>2,17</sup> This is the situation in the Cu barrier pin wire, as sketched in Fig. 5(a). It can be shown<sup>2</sup> that in the one-dimensional case, with the simplest boundary conditions, the energy of the  $n$ th bound state is given by

$$\frac{2d_N}{\hbar v_F} E_n = n\pi + \cos^{-1} \left( \frac{E_n}{\Delta_p} \right), \quad (2)$$

where  $\Delta_p$  is the pair potential,  $d_N$  is the width of the normal region, and  $v_F$  is the normalized Fermi velocity in  $N$ . Figure 5(b) depicts two differential conductance curves taken on the wire with the Cu barrier pin, sample C, over the Cu near the Cu-NbTi boundary. The first curve was acquired in the middle of a hexagon's side while the other was acquired near a hexagon's corner, as illustrated in Fig. 5(a). We see that both curves have almost the same gap and manifest a subgap structure, which we attribute to quasiparticle bound states. It should be noted that the curves taken in the middle of a hexagon's side (such as curve 1) exhibit a sharper and somewhat higher energy of the bound state than the curves taken at the hexagon's corner (such as curve 2). The reason for this may be that at the corner of the hexagon  $d_N$  is not as well defined as in the middle of a side section. Furthermore, while the bound state in curve 1 results predominantly from Andreev reflections *perpendicular* to the Cu channel, those in curve 2 have large contributions from reflections of quasiparticles traversing *along* the Cu channel, as well as from reflections from the hexagon corners. These lead to both broadening and lowering of the bound states in the corner (2) position. The energy location of the subgap features are somewhat lower, although in reasonable agreement with that predicted by Eq. (2) for our sample's parameters. We wish to note that despite these spatial variations in the detailed shape of the subgap structure, such structures (the bound states) have been found *only inside* the Cu region. Moreover, even there, they could be resolved only in the vicinity of the S-N boundaries, since deeper inside the Cu the superconductor

gap in the DOS diminishes and overlaps the bound state. However, wherever it can be detected, the energy of the subgap structure does not depend on the distance from the  $N$ - $S$  boundary.

### SUMMARY

In this article we have demonstrated that detailed information on the PE can be obtained by employing STM in spatially resolved measurements where tunneling is parallel to the  $N$ - $S$  boundaries. The spatial variations of superconductivity as a function of distance from  $N$ - $S$  interfaces in various APC superconducting wires were investigated, and two major results were found: (1) The healing length of superconductivity inside  $S$  (NbTi) is much longer than the Ginzburg-Landau coherence length,  $\xi_S$ . This can possibly be attributed to the effects of both material intermixing and local magnetic fields. It may also be due to weakening of the pair potential in NbTi near the  $N$ - $S$  interface, affecting the spatial variations of the DOS (2) A gap develops in the DOS of the  $N$  metal, at distances from the  $S$ - $N$  boundary which are consistent with the dirty-limit approximation. A

more accurate theoretical modeling using Usadel equations is needed in order to better understand the evolution of the DOS on both sides of the  $N$ - $S$  interface. Up to now Usadel formalism has been applied only for simple geometries, such as a single  $N$ - $S$  interface<sup>5,6</sup> or PE in narrow constrictions,<sup>11,21</sup> and the implementation to our geometry is unfortunately not straightforward. Finally, we found (at specific STM tip positions) pronounced subgap structures in the  $I$ - $V$  characteristics due to quasiparticle bound states, as well as above-gap structure, attributed to Tomasch oscillations. To the best of our knowledge, these effects have not been measured in a configuration where the tunneling current is *parallel* to the materials' interfaces, namely, perpendicular to the path of the Andreev-reflected quasiparticles. Such measurements directly depict the effect of Andreev reflections on the local DOS.

### ACKNOWLEDGMENT

The research at Yale and IGC was supported by the State of Connecticut, NSF-DMR and IGC-AS.

\*Electronic address: milode@vms.huji.ac.il

†Present address: NIST 814.05 Boulder, CO 80303.

<sup>1</sup>G. Deutscher and P. G. de Gennes, in *Superconductivity*, edited by R. D. Parks (Dekker, New York, 1969), Vol. 2.

<sup>2</sup>E. L. Wolf, *Principles of Electron Tunneling Spectroscopy* (Oxford University Press, Oxford, 1989).

<sup>3</sup>P. G. de Gennes, *Superconductivity of Metals and Alloys* (Benjamin, New York, 1966).

<sup>4</sup>K. D. Usadel, Phys. Rev. Lett. **25**, 507 (1970).

<sup>5</sup>S. Gueron, H. Pothier, N. O. Birge, D. Esteve, and M. H. Devoret, Phys. Rev. Lett. **77**, 3025 (1996).

<sup>6</sup>W. Belzig, C. Bruder, and G. Schoen, Phys. Rev. B **54**, 9443 (1996).

<sup>7</sup>R. C. Dynes, V. Naraynamurti, and J. P. Garno, Phys. Rev. Lett. **41**, 1509 (1978).

<sup>8</sup>A. C. Mota, P. Visani, A. Pollini, and K. Aupke, Physica B **197**, 95 (1994).

<sup>9</sup>L. Capogna and M. G. Blamire, Phys. Rev. B **53**, 5683 (1996).

<sup>10</sup>H. Courtois, Ph. Gandit, D. Maillly, and B. Pannetier, Phys. Rev. Lett. **76**, 130 (1996).

<sup>11</sup>B. A. Aminov, A. A. Golubov, and M. Yu. Kuprianov, Phys. Rev. B **53**, 365 (1996).

<sup>12</sup>S. H. Tessmer, D. J. Van Harlingen, and J. W. Lyding, Phys. Rev. Lett. **70**, 3135 (1993); S. H. Tessmer, M. B. Tarlie, D. J. Van Harlingen, D. L. Maslov, and P. M. Goldbart, *ibid.* **77**, 924 (1996).

<sup>13</sup>J. Wildoer, Ph.D. thesis, TU Delft, 1996.

<sup>14</sup>H. F. Hess, R. B. Robinson, R. C. Dynes, J. M. Valles, Jr., and J. V. Waszczak, Phys. Rev. Lett. **62**, 214 (1989); H. F. Hess, R. B. Robinson, R. C. Dynes, J. M. Valles, Jr., and J. V. Waszczak, J. Vac. Sci. Technol. A **8**, 450 (1990).

<sup>15</sup>K. Inoue and H. Takayanagi, Phys. Rev. B **43**, 6214 (1991).

<sup>16</sup>Y. Levi, O. Millo, N. D. Rizzo, D. E. Prober, and L. R. Motowidlo, Appl. Phys. Lett. **72**, 480 (1998).

<sup>17</sup>P. G. de Gennes and D. Saint James, Phys. Lett. **4**, 151 (1963).

<sup>18</sup>W. J. Tomasch, Phys. Rev. Lett. **15**, 672 (1965).

<sup>19</sup>L. R. Motowidlo, B. A. Zeitlin, M. S. Walker, and P. Haldar, Appl. Phys. Lett. **61**, 991 (1992); N. D. Rizzo, J. Q. Wang, D. E. Prober, L. R. Motowidlo, and B. A. Zeitlin, *ibid.* **69**, 2285 (1996).

<sup>20</sup>R. W. Heussner, J. D. Marquandt, P. J. Lee, and D. C. Larbales-tier, Appl. Phys. Lett. **70**, 901 (1997).

<sup>21</sup>A. A. Golubov, F. K. Wilhelm, and A. D. Zaikin, Phys. Rev. B **55**, 1123 (1997).

<sup>22</sup>X. S. Ling, J. D. McCambridge, N. D. Rizzo, J. W. Sleight, D. E. Prober, L. R. Motowidlo, and B. A. Zeitlin, Phys. Rev. Lett. **74**, 805 (1995).

<sup>23</sup>R. O'Barr, M. Lederman, S. Schultz, W. Xu, A. Scherer, and R. J. Tonucci, J. Appl. Phys. **79**, 5303 (1996).

<sup>24</sup>J. Q. Wang, N. D. Rizzo, D. E. Prober, L. R. Motowidlo, and B. A. Zeitlin, IEEE Trans. Appl. Supercond. **7**, 1130 (1997).

<sup>25</sup>J. Aarts, J. M. E. Geers, E. Bruk, A. A. Golubov, and R. Coehoorn, Phys. Rev. B **56**, 2779 (1997).